ACS OMEGA

Open Access

http://pubs.acs.org/journal/acsodf

Article

Modulation of $[CuOH/O]^+$ Properties in $[2,2'\text{-Bipyridine}]_2$ Homoleptic Complexes through Substitution at the 6,6′ Position by Methyl Groups

Alessandro Damin,* Matteo Bonomo, Barbara Centrella, Matteo Signorile, Claudia Barolo, and Silvia Bordiga

Cite This: *ACS Omega* 2024, 9, 16610−16620

Read Online

ACCESS | Metrics & More | Article Recommendations | Supporting Information

ABSTRACT: In this paper, data from a DFT-based computational study on the reactivity of $[Cu(2,2'\text{-}\boldsymbol{S}\text{-bpy})_2]^+PF6^-$ (***S*** indicating substitution by methyl groups at the 6 and/or 6′ position and ranging from 0 to 100% through 50%) homoleptic complexes based toward tButOOH were presented. Computational results, supported by cyclic voltammetry analysis, prove the feasibility of finely tuning the chemical properties of the complexes and their reactivity by means of insertion of methyl moieties in selected positions within the bipyridine scaffold.

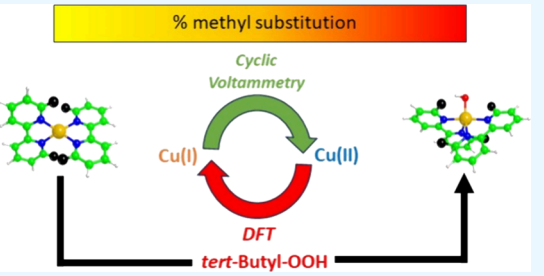

INTRODUCTION

2,2′-Bipyridine (hereafter bpy) molecules represent an important class of ligands through which properties of coordinating transition metal (e.g., Cu) can be finely tuned, for instance, by altering the substituent groups at the 6 and/or 6′ position (2,2′-***S***-bpy). As a matter of fact, as it clearly emerged from the analysis of literature data concerning light-emitting electrochemical cells,[1−3] the $E_{1/2}$ of heteroleptic complexes of general formula $[Cu(2,2'\text{-}\boldsymbol{S}\text{-bpy})\text{-xantphos}]^+[PF_6]^-$ varies from +760 to +890 mV vs Fc/Fc^+, through +850 mV vs Fc/Fc^+ (= −5.1 eV vs vacuum), on passing from $[Cu(2,2'\text{-bpy})\text{xantphos}]^+[PF_6]^-$ (***S*** = 0) to $[Cu(2,2'\text{-}\boldsymbol{6,6'\text{-}Me_2}\text{-bpy})\text{xantphos}]^+[PF_6]^-$ (***S*** = ***6,6′-Me***$_2$), through $[Cu(2,2'\text{-}\boldsymbol{6\text{-}Me}\text{-bpy})\text{xantphos}]^+[PF_6]^-$ (***S*** = ***6-Me***) and with Me = $-CH_3$.[3] The same behavior was observed for the $[Cu(2,2'\text{-}\boldsymbol{S}\text{-bpy})POP]^+[PF_6]^-$ class of compounds (POP = bis(2-(diphenylphosphanyl)phenyl)ether).[3] On passing to the well-known homoleptic complex $[Cu(2,2'\text{-}\boldsymbol{6,6'\text{-}Me_2}\text{-bpy})_2]^+[PF_6]^-$, this showed very high performance as a redox mediator in dye-sensitized solar cells, the main reason being attributed to the low reorganization (flattening) occurring when the complex is reversibly oxidized to the $[Cu(2,2'\text{-}\boldsymbol{6,6'\text{-}Me_2}\text{-bpy})_2]^{2+}[PF_6]^-$ form compared to structural analogues (e.g., $[Cu(2,2'\text{-bpy})_2]^{2+}[PF_6]^-$), which is possibly due to steric hindrance from Me substituent groups at the 6,6′ position.[4]

It was recently shown by some of us[5] that such a feature can be exploited to employ the $[Cu(2,2'\text{-}\boldsymbol{6,6'\text{-}Me_2}\text{-bpy})_2]^+[PF_6]^-$ system (measured $E_{1/2}$ = 697 mV vs Ag^+/Ag) as an active catalyst for allylic oxidation of cyclohexene by *tert*-butyl-hydroperoxide (hereafter tBuOOH) in CH_2Cl_2 (hereafter DCM) solutions; in fact, when contacted by tBuOOH, $[Cu(2,2'\text{-}\boldsymbol{6,6'\text{-}Me_2}\text{-bpy})_2]^+[PF_6]^-$ transforms to oxidated species where Cu^+ passes to Cu^{2+}, bearing OH/O groups that can be subsequently transferred to cyclohexene causing the back-reduction of the oxidated complex to the original form containing Cu^+. It is worth mentioning here that such a redox cycle was not observed for the $[Cu(2,2'\text{-bpy})_2]^+[PF_6]^-$ system (measured $E_{1/2}$ = 269 mV vs Ag^+/Ag) and oxidation by tBuOOH resulted in a quite fast but irreversible oxidative process, no back-reduction being observed after contacting with cyclohexene, so suggesting that $[Cu(2,2'\text{-bpy})_2]^+[PF_6]^-$ cannot be adopted as a useful catalytic system.

On the other hand, the good reversibility observed for $[Cu(2,2'\text{-}\boldsymbol{6,6'\text{-}Me_2}\text{-bpy})_2]^+[PF_6]^-$ that is ascribable to the substituting methyl groups was accompanied by a quite high slowness in the oxidation process (2 h was required for the whole Cu^+/Cu^{2+} conversion when a Cu:tBuOOH = 1:60 molar ratio is adopted), so strongly affecting its catalytic performances. Notice that from previous calculations[5] (see also the data below reported), thermodynamics features characterizing the Cu(I) + tBuOOH → Cu(II)OH + tBuO reaction resulted to be (when $[Cu(2,2'\text{-}\boldsymbol{6,6'\text{-}Me_2}\text{-bpy})_2]^+[PF_6]^-$ is involved) unfavorable (computed $\Delta G^{298K} > 0$), so in partly explaining why the oxidation process resulted to be so difficult to occur.

Received: January 18, 2024
Revised: January 31, 2024
Accepted: February 2, 2024
Published: March 29, 2024

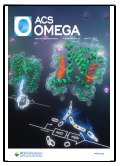

Based on these data, it is quite clear how the degree of substitution would impact on the likeness of the oxidation process as well as on its kinetic. As such, the modulation of the number of methyl moieties on the bipyridine ligands is expected to impact on the electrochemical potential of the Cu center due to both steric (i.e., geometrical) and electronic effects. Therefore, a possible way to control both the fastness in the oxidation process and its reversibility could rely on the modulation of the degree of methyl group substitution, i.e., by employing as ligands the bipyridine molecule substituted by a single methyl group just at the 6 position. Notice that the $[Cu(2,2'\text{-}\mathbf{6}\text{-}\mathbf{Me}\text{-bpy})_2]^+[PF_6]^-$ complex was already synthesized[6] but nothing has been done concerning its reactivity toward tButOOH nor its catalytic activity in oxygenation of alkenes. To get some preliminary insights about its behavior in oxidation processes and how it behaves with respect to $[Cu(2,2'\text{-bpy})_2]^+[PF_6]^-$ and $[Cu(2,2'\text{-}\mathbf{6,6'}\text{-}\mathbf{Me_2}\text{-bpy})_2]^+[PF_6]^-$, we initially performed a systematic computational study of energetics features (namely, the redox potential) of homoleptic $[Cu(2,2'\text{-}\mathbf{S}\text{-bpy})_2]^+[PF_6]^-$ complexes (where S = 0, 6-Me, and 6,6′-Me_2 for a final %Me substitution of 0, 50, and 100%, respectively). Good agreement with experimental results (as from cyclic voltammetry analysis), which shows an almost perfectly linear correlation (R^2 = 0.997) between the measured $E_{1/2}$ and the percentage of methyl group substitution and a good reversibility of the $[Cu(2,2'\text{-}\mathbf{6}\text{-}\mathbf{Me}\text{-bpy})_2]^+[PF_6]^-$ system, encouraged us to extend the computational investigation, through the same methodology, to the reactivity of the latter toward the tButOOH oxidant agent too. As it will be shown in the following, the computed thermodynamics features suggest that the reaction between $[Cu(2,2'\text{-}\mathbf{6}\text{-}\mathbf{Me}\text{-bpy})_2]^+[PF_6]^-$ and tButOOH to form −Cu(OH/O) species can occur more easily than when $[Cu(2,2'\text{-}\mathbf{6,6'}\text{-}\mathbf{Me_2}\text{-bpy})^2]^+[PF_6]^-$ is involved, possibly eliminating the observed drawbacks (at least when the thermodynamics of the process is considered) occurring in the catalytic activity of the latter toward the oxygenation of alkenes.

RESULTS AND DISCUSSION

Homoleptic complexes [Cu(2,2′-**S**-bpy)2]$^+$[PF6]$^-$ were modeled by adopting the CuBP-X_mY_n cluster model (see Figure 1 for a graphical representation), including the PF_6^- counterion and implicit DCM model solvent through the whole set of calculations.

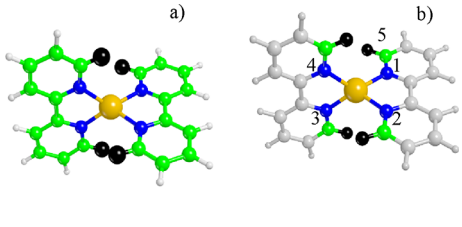

Figure 1. (a) Graphical representations of CuBP-X_mY_n (m/n = 0/4, m/n = 2/2, m/n = 4/0) optimized molecular models where black spheres show X = Me and Y = H. For CuBP-Me_2H_2, methyl groups substitute the black spheres on the N1 and N4 side. White, green, blue, and orange spheres show H, C, N, and Cu atoms, respectively. The PF_6^- counterion is omitted for the sake of clarity. (b) The same as in part (a) but with Cu first and second neighbors underlined by colored spheres (color code as in part a). Numbers show the atoms with respective geometrical features taken. Gray spheres represent the remaining part of the complex.

Geometrical features of the optimized models (*xyz* coordinates listed in the Supporting Information, points A, B, and C) are reported in Table 1, and as can be seen from the reported data, they are not significantly affected by the percentage of Me (%Me) substitution (0, 50, and 100 for CuBP-Me_0H_4, CuBP-Me_2H_2, and CuBP-Me_4H_0, respectively), the three models being characterized by a flattened tetrahedron (pseudo-D_2 symmetry) configuration. As it clearly appears from Figure 1, in the adopted models, the Cu-chelating bpy molecules are both in their *cis* conformer so that the four N atoms are pointing toward the metal ion. This should be the preferred orientation in terms of electrostatics because it maximizes the dipole−charge interaction between the copper ion and dipole characterizing the pyridine ring. In fact, this is the structure that CuBP-Me_2H_2[6] and CuBP-Me_4H_0[7] retain in their solid phase. Test calculations performed on $CuBP^{cis}BP^{trans}$-Me_2H_2, i.e., where one of the two chelating bpy molecules assumes the *trans* conformation (*xyz* coordinates of the optimized structure are listed in the Supporting Information, point B8), strongly suggest that this is the same structure that the complexes have in solution: in fact, the latter resulted to be less stable than CuBP-Me_2H_2 of 31.0 kJ mol^{-1}. Also, the strong similarities observed between the Raman spectra recorded on dichloromethane solution and on the solid phase of the $[Cu(2,2'\text{-}\mathbf{6,6'}\text{-}\mathbf{Me_2}\text{-bpy})_2]^+[PF_6]^-$ complex[5] are in favor to the findings from calculations. It is worth noticing here that the computed Raman spectra on CuBP-Me_2H_2/CuBP-Me_4H_0 models (see purple/navy solid lines in Figure S1, part a) reproduce quite well not only the major vibrational features experimentally observed (obtained on DCM solution of $[Cu(2,2'\text{-}\mathbf{6}\text{-}\mathbf{Me}\text{-bpy})_2]^+[PF_6]^-$/$[Cu(2,2'\text{-}\mathbf{6,6'}\text{-}\mathbf{Me_2}\text{-bpy})_2]^+[PF_6]^-$, see purple/navy solid lines in Figure S1, part b) but also the relative observed changes occurring between the two complexes.

The UV−vis spectra (see Figure S2) computed on the optimized CuBP-Me_0H_4, CuBP-Me_2H_2 (PF_6 moiety in the *cis* position with respect to $-H_2$), and CuBP-H_0Me_4 cluster models show the presence of an intense signal with a maximum decline, respectively, at 20,447, 20,422, and 20,932 cm^{-1} that is assignable to MLCT (metal to ligand charge transfer) characterizing the experimental UV−vis spectra of $[Cu(2,2'\text{-bpy})_2]^+[PF_6]^-$ and $[Cu(2,2'\text{-}\mathbf{6,6'}\text{-}\mathbf{Me_2}\text{-bpy})_2]^+[PF_6]^-$ recorded in DCM (near 22,000 cm^{-1} in both cases).[5] The reported values prove that the Me substitution just slightly affects the position of MLCT.

Before passing to the study of the interaction of CuBP-X_mY_n with tButOOH, it is useful to briefly discuss here the thermodynamics (energetics) behavior of such complexes toward monoelectronic oxidation. For the three CuBP-Me_0H_4, CuBP-Me_2H_2, and CuBP-Me_4H_0 complexes, the computed $\Delta G_{red}^{298K}(\Delta E_{red})$ resulted to be −460.0(−441.9), −492.3(−471.0), and −514.9(−484.8) kJ mol^{-1}, respectively (see the Theoretical Basis Section for the definition of ΔG_{red}^{298K}). The optimized structures (*xyz* coordinates listed in the Supporting Information, points A1, B1, and C1) do not show too much distortion from those containing a Cu(I) center, except for further flattening, this being in line with the tendency of Cu(II) to reach a square planar coordination, which is particularly evident when CuBP-Me_0H_4 is considered where steric hindrance from Me groups is not present. In particular, τ (i.e., the torsion angle defining the rotation of bipyridine molecules around an axis containing the points at average distance between N3−N4 and N1−N2 as defined in

https://doi.org/10.1021/acsomega.4c00598
ACS Omega 2024, 9, 16610−16620

Table 1. Geometrical Features (Cu−N_i = Distances, N_i−Cu−N_j = Angles) of the Optimized CuBP-X_mY_n Molecular Models[a]

X_mY_n	Cu−N_1	Cu−N_2	Cu−N_3	Cu−N_4
Me_0H_4	2.035	2.050	2.037	2.038
Me_2H_2	2.038	2.040	2.030	2.036
Me_4H_0	2.027	2.052	2.053	2.027

X_mY_n	N_1−Cu−N_2	N_3−Cu−N_4	N_1−Cu−N_4	N_2−Cu−N_3	N_1−Cu−N_3	N_2−Cu−N_4
Me_0H_4	80.9	81.2	128.6	122.7	128.0	121.4
Me_2H_2	81.0	81.4	124.5	125.2	128.0	122.9
Me_4H_0	81.3	81.3	137.6	120.6	120.6	120.7

[a]X = Me, Y = H. *i*, *j* = 1−4 as defined in Figure 1b. Distances and angles are expressed in Å and degrees (deg), respectively.

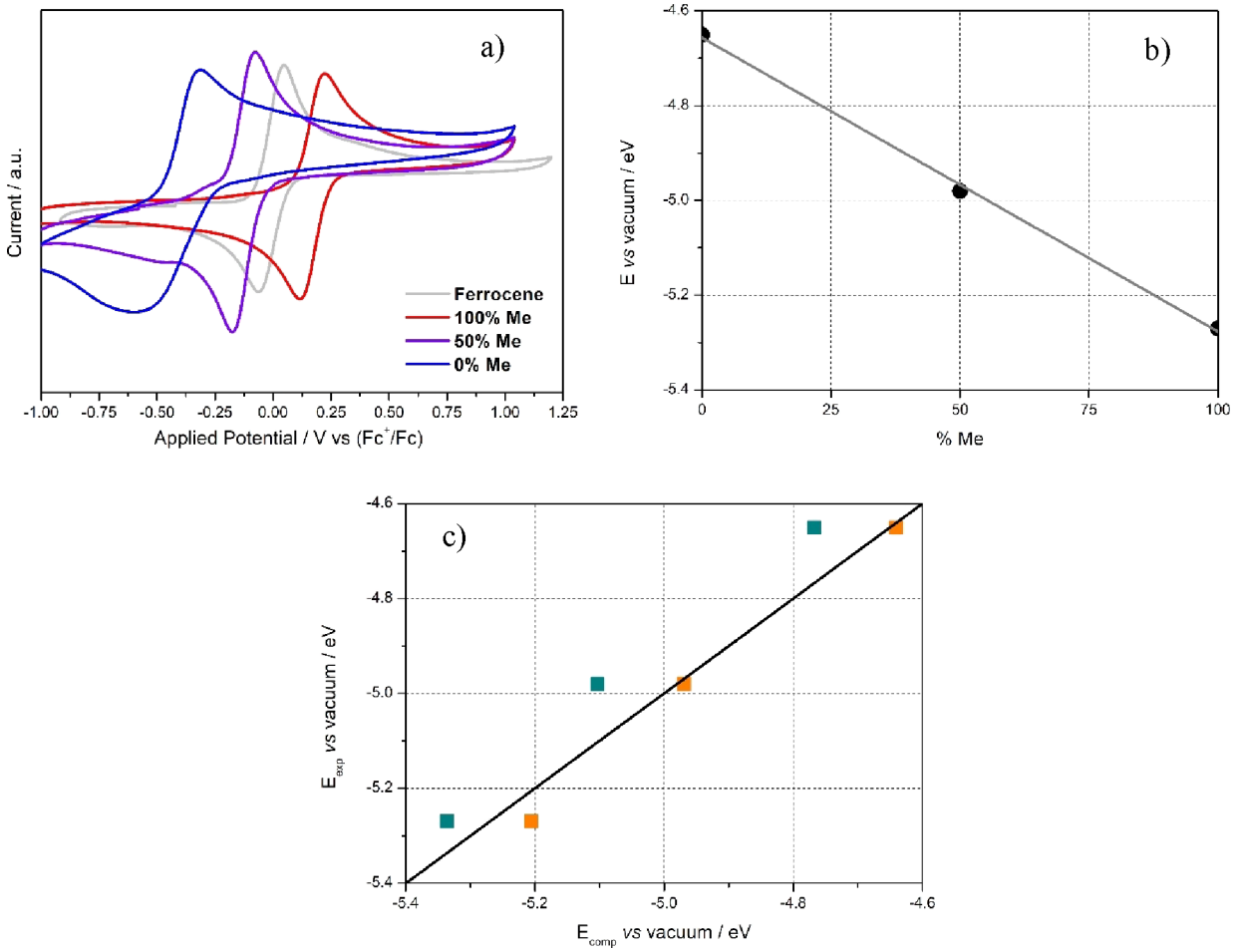

Figure 2. (a) Cyclic voltammogram curves obtained on CuBP-X_mY_n (m/n = 0/4, 2/2, and 4/0, respectively, for 100% Me, 50% Me, and 0% Me) complexes in DCM solution and vs ferrocene. (b) Reduction potential E vs vacuum plotted against % Me substitution (solid black circles). The gray line shows the linear fitting (adjusted R^2 = 0.997, slope = −0.006 eV/%Me) of the reported data. (c) Comparison between computed E [eV] vs vacuum (E_{comp}) and experimental E [eV] vs vacuum (E_{exp}). $E_{comp} = \Delta G_{red}^{298K} \times 0.010364$ eV mol/kJ. Dark cyan squares represent the values obtained by ΔG_{red}^{298K} (see the Theoretical Basis Section for further details). Orange solid squares show the values obtained from ${}^{drc}\Delta G_{red}^{298K}$ (see Theoretical Basis Section for further details).

Figure 1, part b) show decreases of 50.8, 38.9, and 20.3° for CuBP-Me_0H_4 (initial value of 91.0°), CuBP-Me_2H_2 (initial value of 91.0°), and CuBP-Me_0H_4 (initial value of 83.5°), respectively. When the origin of the obtained thermodynamics (energetics) trend is of concern, the effect of Me substitution on some global reactivity indexes (e.g., ionization potential (IP), electron affinity (EA), and electronegativity (χ), which is defined as the arithmetical average of IP and EA)[8,9] characterizing the adopted Cu ligands (i.e., BP-Me_0H_4, BP-M_2H_2 and BP-Me_4H_0 in *cis* conformation) was investigated too. The results showed that χ underwent a systematic decrease along the BP-Me_0H_4, BP-Me_2H_2, and BP-Me_4H_0 series (406.0, 395.2, and 385.9 kJ mol^{-1}, respectively), suggesting that steric hindrance from Me substitution can only in part explain the observed thermodynamics (energetics) trend.

The easiness in the oxidation of the metal center could be likely related to its reduction potential. The higher the reduction potential is, the higher the energy required to oxidize Cu(I) to Cu(II), needing a more powerful oxidant. The data summarized in Figure 2 confirmed the observation already reported for CuBP-Me_4H_0 (solid red line in Figure 2,

https://doi.org/10.1021/acsomega.4c00598
ACS Omega 2024, 9, 16610−16620

part a) and CuBP-Me_0H_4 (solid blue line in Figure 2, part a) in our previous paper, with the former showing a much higher reduction potential (+0.17 V vs Fc^+/Fc) compared to the latter (−0.45 V vs Fc^+/Fc).

Moreover, CuBP-Me_4H_0 shows a very good reversibility (ΔE = 0.10 V), whereas the reduction peak of CuBP-Me_0H_4 is clearly broadened (ΔE = 0.27 V). This phenomenon was associated with the practically null solubility of Cu(II)BP-Me_0H_4 that tends to precipitate as soon as it is formed, as also proven by the formation of green crystallites at the bottom of the vial. As predicted by computational analysis, CuBP-Me_2H_2 (synthesized according to the procedure described in the Materials and Methods Section and characterized through NMR spectroscopy, see Figure S3) shows a reduction potential (−0.12 V vs Fc^+/Fc, also characterized by a very good reversibility, ΔE = 0.10 V) placed almost perfectly at the halfway point (solid violet line in Figure 2, part a) between the other two considered homoleptic complexes, so obtaining a good linear correlation (see part b of Figure 2) of E (reducing potential obtained vs vacuum) against %Me substitution; this further proves how the electrochemical potential of a complex could be finely tuned by specific chemical modification of the ligand. It is interesting to notice here that computed values E_{comp} (derived from calculated ΔG_{red}^{298K}, see the Theoretical Basis Section for further details) are in very good agreement with the experimental ones (E_{exp}, see part c of Figure 2).

On passing now to the reactivity of CuBP-X_mY_n cluster models with tButOOH, graphical representations of the reacted clusters (Cu(OH/O)BP-X_mY_n) along (reaction 1)$_{DCM}$ (*xyz* coordinates of the optimized structures are listed in the Supporting Information, points A2, B2, and C2) and (reaction 2)$_{DCM}$ (*xyz* coordinates of the optimized structures are listed in the Supporting Information, points A3, B3, and C3) are reported in Figure 3, and as can be clearly observed,

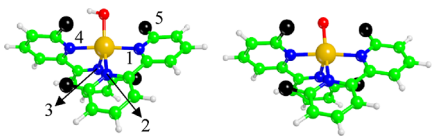

Figure 3. Graphical representations of Cu(OH/O)BP-X_mY_n (m/n = 0/4, 2/2, and 4/0) optimized molecular models where black spheres show X = Me and Y = H. White, green, blue, red, and orange spheres show H, C, N, O, and Cu atoms, respectively. The PF_6^- counterion is omitted for the sake of clarity.

strong deformation with respect to CuBP-X_mY_n occurs. For the m/n = 2/2 case, the same general structures as those reported in Figure 2 are obtained, regardless of what OH/O moieties occupy the *cis* position with respect 2 Me groups (Cu(OH/O)-Me_2H_2) to 2 H groups (Cu(OH/O)-H_2Me_2, *xyz* coordinated listed at points B4 and B5 of the Supporting Information) and to Me and H groups (Cu(OH/O)-MeHMeH, *xyz* coordinate listed at points B6 and B7 of the Supporting Information).

The geometrical features of the Cu(OH)BP-X_mY_n and Cu(O)BP-X_mY_n optimized models are reported in Table 2 and Table 3, respectively. For the $m/2$ = 2/2 case, just features for the Cu(OH/O)-Me_2H_2 optimized structures are reported.

As can be seen, the N_1−Cu−N_4 angle (see Figure 1 for its definition) resulted to be the most affected, being quite near to 180° independent from the % of Me substitution in the three considered systems. The Cu−O distance falls in the 1.897−1.917 Å range for Cu(OH)BP-X_mY_n models, in a range quite near to the experimentally observed[10] value and with the Cu−OH angle located at 109.0°; Cu−O resulted instead to be slightly shorter (1.868−1.886 Å range) when Cu(O)BP-X_mY_n species are considered.

It is worth noticing here that Me substitution particularly affects the O−Cu−N_1−C_5 torsion angle, which progressively changes from −12.7°/−18.1° to −40.9°/−33.4° on passing from %Me = 0 (Cu(OH/O)-Me_0H_2) to %Me = 100 (Cu(OH/O)-Me_4H_0); intermediate values of −36.5 and −30.0° are obtained for %Me = 50 (Cu(OH)-Me_2H_2 and Cu(O)-Me_2H_2 models respectively). This affects the final coordination sphere of Cu, which can be assumed to be square planar for %Me = 0, taking into account O and the N_1, N_2, and N_4 atoms. When Cu(OH/O)-MeHMeH and Cu(OH/O)-H_2Me_2 models are of concern, it has to be noticed that coordination of Cu quite near to a square planar is obtained; O−Cu−N_1−C_5 torsion angles are, respectively, 19.5°/21.0° and −18.4°/−20.9°.

The comparison between Figure S2 (UV−vis spectra computed for CuBP-X_mY_n pristine models) and those obtained on tButOOH reacted models (see Figure 4 and Figure 5) clearly shows that the resulting Cu(OH/O)BP-X_mY_n species possess quite different electronic features with respect to CuBP-X_mY_n pristine ones. In particular, the results show a quite evident erosion of the intense MLCT band and the growth of much weaker signals at higher and lower wavenumbers. As far as the CuBP-Me_4H_0 system is concerned, after reaction with tBuOOH and the consequent formation of Cu(OH)BP-Me_4H_0 species, the MLCT band is substituted by bands with maxima located at 25,781, 14,508, and 10,420 cm^{-1}, the former being the most intense one (see the solid blue line in Figure 4, part a).

Table 2. Geometrical Features (Cu−N_i, Cu−O = Distance, O−Cu−N_i−C_l = Dihedral Angle, N_i−Cu−N_j = Angle) of the Optimized Cu(OH)BP-X_mY_n Molecular Models[a]

X_mY_n	Cu−N_1	Cu−N_2	Cu−N_3	Cu−N_4	Cu−O	O−Cu−N_1−C_5
Me_0H_4	2.025	2.056	2.314	2.047	1.897	−12.7
Me_2H_2	2.066	2.042	2.228	2.071	1.910	−36.5
Me_4H_0	2.034	2.124	2.277	2.041	1.917	−40.9
X_mY_n	N_1−Cu−N_2	N_3−Cu−N_4	N_1−Cu−N_4	N_2−Cu−N_3	N_1−Cu−N_3	N_2−Cu−N_4
Me_0H_4	79.6	76.2	175.2	88.9	105.3	95.9
Me_2H_2	80.1	77.0	174.3	98.2	103.0	94.2
Me_4H_0	80.4	77.6	174.8	100.4	106.5	102.2

[a]X = Me, Y = H. *i*, *j* = 1−4 and *l* = 5 as defined in Figure 1b. Distances, dihedral angles, and angles are expressed in Å, degrees (deg), and degrees (deg), respectively.

https://doi.org/10.1021/acsomega.4c00598
ACS Omega 2024, 9, 16610−16620

Table 3. Geometrical Features (Cu−N_i, Cu−O = Distance, O−Cu−N_i−C_l = Dihedral Angle, N_i−Cu−N_j = Angle) of the Optimized Cu(O)BP-X_mY_n Molecular Models[a]

X_mY_n	Cu−N_1	Cu−N_2	Cu−N_3	Cu−N_4	Cu−O	O−Cu−N_1−C_5
Me_0H_4	2.010	2.059	2.263	2.061	1.868	−18.1
Me_2H_2	2.059	2.043	2.229	2.063	1.872	−30.0
Me_4H_0	2.034	2.091	2.246	2.062	1.886	−33.4
X_mY_n	N_1−Cu−N_2	N_3−Cu−N_4	N_1−Cu−N_4	N_2−Cu−N_3	N_1−Cu−N_3	N_2−Cu−N_4
Me_0H_4	80.1	76.2	173.2	93.6	109.5	96.1
Me_2H_2	80.4	77.7	174.8	98.7	100.9	94.8
Me_4H_0	80.8	77.3	168.3	101.3	114.1	99.9

[a]X = Me, Y = H. *i*, *j* = 1−4 and *l* = 5 as defined in Figure 1b. Distances, dihedral angles, and angles are expressed in Å, degrees (deg), and degrees (deg), respectively.

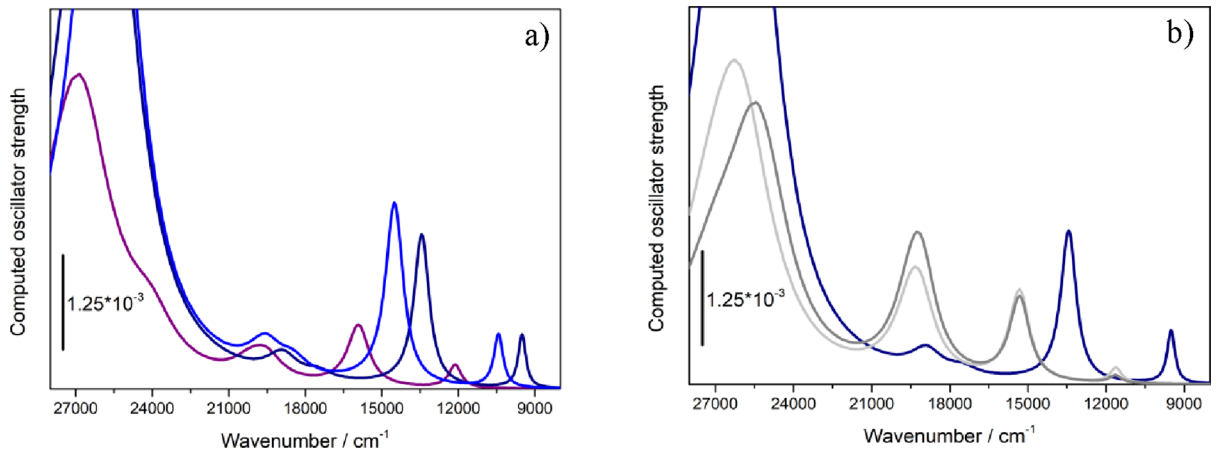

Figure 4. (a) UV−vis spectra computed for Cu(OH)BP-X_mY_n complexes (X = Me, Y = H). Purple solid line: m/n = 0/4. Navy solid line: m/n = 2/2. Blue solid line: m/n = 4/0. (b) UV−vis spectra computed for Cu(OH)BP-MeHMeH and Cu(OH)BP-H_2Me_2 complexes (dark gray and light gray solid lines, respectively). UV−vis spectrum computed for Cu(OH)BP-Me_2H_2 (navy solid line) is also reported for the sake of comparison.

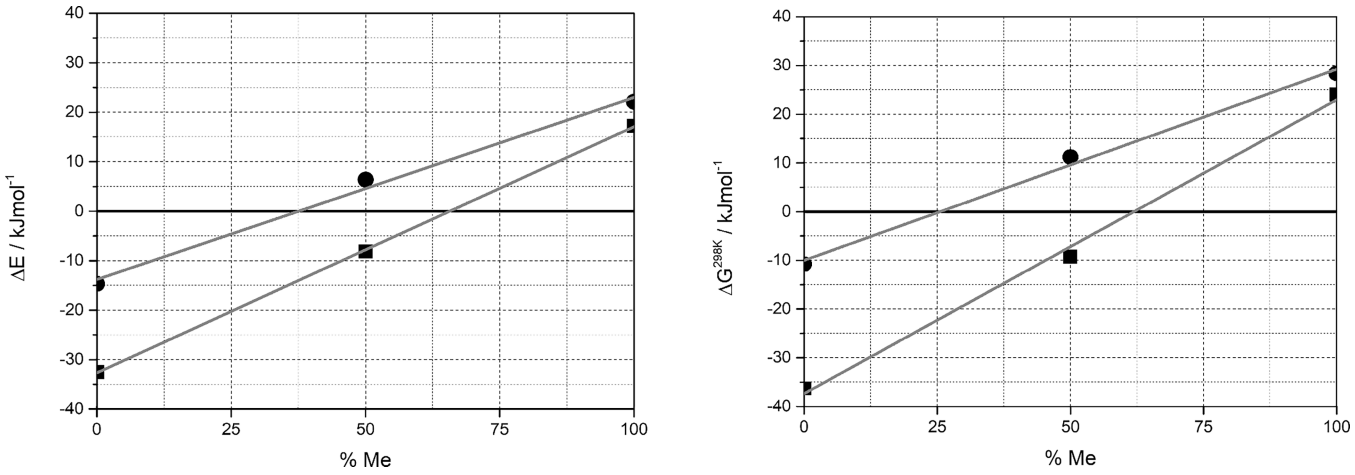

Figure 5. ΔE and ΔG^{298K} vs %Me (percentage Me substitution) computed for (reaction 1)$_{DCM}$ (solid squares) and (reaction 2)$_{DCM}$ (solid circles) involving the CuBP-(Me_0H_4, Me_2H_2, Me_4H_0) molecular models. Dark gray lines show the linear fitting results (data from fitting are reported in Table S2).

Notice that this is the same behavior showed experimentally[5] by the $[Cu(2,2'$-***6,6'-Me*$_2$-bpy$)_2]^+[PF_6]^-$ system after reaction with tButOOH: the two bands at 14508 and 10420 cm^{-1} (quite near to those experimentally observed) are ascribable to transitions mainly involving the Cu center and possessing a prevalent "d−d" character. This observation along with the analysis of computed Mulliken spin densities (ρ) for Cu and OH centers (ρ_{Cu} = 0.659 *e* and ρ_{OH} = 0.169 *e*) leads to the conclusion that $[Cu^{2+}(OH)^-]^+$ species are obtained after the reaction of CuBP-Me_4H_0 with tButOOH, a situation that is quite far from what was obtained for isolated $[CuOH]^+$, where the $[Cu^+(OH)^{\cdot}]^+$ configuration appeared to be the predominant one (even if a partial $Cu^{2+}(OH)^-$ character of the bond cannot be excluded) and much closer to what was observed for its hydrated counterpart.[11] The computed UV−vis spectrum for the Cu(OH)BP-Me_0H_4 system (see the purple line in Figure 4) shows approximately the same features as those above-discussed, but some noticeable differences can be

https://doi.org/10.1021/acsomega.4c00598
ACS Omega 2024, 9, 16610−16620

observed: in fact, "d−d" bands resulted to be blue-shifted (being now located at 15,904 and 12,096 cm^{-1}) and of much lower intensity when compared to what was obtained for Cu(OH)BP-Me_4H_0, this presumably being ascribable to the square planar coordination (characterized by a higher ligand field and higher symmetry) that the Cu species reached in the optimized Cu(OH)BP-Me_0H_4 system. Also in this case, spin density analysis confirmed that $[Cu^{2+}(OH)^-]^+$ species are obtained (ρ_{Cu} = 0.645 *e* and ρ_{OH} = 0.157 *e*). Moreover, the presence of a band with a maximum located at 26,897 cm^{-1} (quite near to what was obtained for Cu(OH)BP-Me_4H_0) but characterized by a much lower intensity can be observed.

When the UV−vis spectra computed for %Me = 50 derived systems are of concern (navy solid line in Figure 3, part a and b, and dark gray and light gray solid lines in Figure 4, part b), two main situations can be observed, possibly reflecting the different coordination that the Cu atom reached in Cu(OH)-BP-Me_2H_2 and Cu(OH)BP-MeHMeH or Cu(OH)BP-H_2Me_2. In fact, features characterizing the UV−vis spectrum computed for the Cu(OH)BP-Me_2H_2 system, where the O−Cu−N_1−C_5 torsion angle is quite close to that obtained for Cu(OH)BP-Me_4H_0 (see Table 2), resulted in quite similar (in terms of intensity) to those obtained for the latter. In particular, one can notice the presence of two bands ascribable to "d−d" transitions (located now at 13,417 and 9480 cm^{-1}) and a band with a maximum located at 26,135 cm^{-1}.

The analysis of spin densities for Cu and OH moieties of the Cu(OH)BP-Me_2H_2 system showed that ρ_{Cu} = 0.669 *e* and ρ_{OH} = 0.142 *e*, indicating that also in this case, $[Cu^{2+}(OH)^-]^+$ species are formed after reaction with tButOOH; their electronic features are quite close to those characterizing the same group in Cu(OH)BP-Me_4H_0, as proven by the comparison of respective computed UV−vis spectra. The analysis of vibrational features confirms once more that the $[Cu(OH)]^+$ species formed at the CuBP-Me_2H_2 complex possess features quite close to those formed from CuBP-Me_4H_0, the computed ν_{Cu-OH} (frequencies associated with the Cu−OH bond stretching) being quite close and centered, respectively, at 476 and 473 cm^{-1}; when the Cu(OH)BP-Me_0H_4 system is of concern, ν_{Cu-OH} resulted instead to be located at 497 cm^{-1}. When Cu(OH)BP-MeHMeH (ρ_{Cu} = 0.651 *e* and ρ_{OH} = 0.181 *e*) and Cu(OH)BP-H_2Me_2 (ρ_{Cu} = 0.640 *e* and ρ_{OH} = 0.185 *e*) are of concern, the main features characterizing the computed UV−vis spectra (see Figure 4, part b) are quite close to what was obtained for the Cu(OH)BP-Me_0H_4 cluster model; this is in accordance with what was already observed for their geometrical features.

Coming now to the energetics features (ΔE) concerning $(\text{reaction 1})_{DCM}$, the data obtained for Cu(OH)BP-Me_0H_4, Cu(OH)BP-Me_2H_2, and Cu(OH)BP-Me_4H_0 are reported in Table 4 and resumed in Figure 5 too (part a, solid black squares); as can be clearly seen, not only %Me substitution affects significantly ΔE, $(\text{reaction 1})_{DCM}$ being highly hexoergonic for Cu(OH)BP-Me_0H_4, but also ΔE showed a quite good linear correlation with %Me (see Table S5 for fitting parameters); dispersive interactions (evaluated through the D3-bj empirical scheme)[12,13] highly contribute in defining the final ΔE ($\Delta E_{D3\text{-}bj}$ of −14.7, −20.1, and −21.2 kJ mol^{-1} were computed for Cu(OH)BP-Me_0H_4, Cu(OH)BP-Me_2H_2, and Cu(OH)BP-Me_4H_0, respectively). It is worth noticing here that ΔE_{el} (evaluated as $\Delta E_{el} = \Delta E - \Delta E_{D3\text{-}bj}$) maintained the same linear correlation with %Me already observed for ΔE (see Figure S5 and Table S3 for fitting parameters). To go much deeper in the origin of the obtained trend, $(\text{reaction 1})_{DCM}$ was decomposed in five possible subreactions according to the path summarized in Table S4, so defining five possible energetics contributions to the final computed ΔE. As it can be seen from the data reported in Table S4, %Me substitution significantly affects not only the energy cost (indicated in Table S4 as ΔE_{def2}) needed for bringing CuBP-X_mY_n to the geometry $[(\text{CuBP-}X_mY_n)_{def}]$ that it has in hydroxylated form but without the −OH group but also the energetics associated with the Cu−OH bond formation (evaluated as ΔE_{int}, see Table S4). Also, on passing to the analysis of thermodynamics features (computed at 298 K), $(\text{reaction 1})_{DCM}$ involving the system with %Me = 0 resulted to be highly favored (ΔG^{298K} = −36.3 kJ mol^{-1}), the system with %Me = 100 being instead characterized by positive ΔG^{298K} located at 24.0 kJ mol^{-1}. Such results can justify (at least from a thermodynamics point of view) the difference in reactivity of the two systems experimentally observed: in fact, $[Cu(2,2'\text{-bpy})_2]^+[PF_6]^-$ reacts instantaneously with tButOOH (Cu:tBUtOOH = 1:1) at variance to what was observed for $[Cu(2,2'\text{-}\boldsymbol{6,6'\text{-}Me_2}\text{-bpy})_2]^+[PF_6]^-$, which took more than 10 h to completely react for the same Cu:tButOOH ratio.

It is worth noticing here that ΔG^{298K} computed for the Cu(OH)BP-Me_2H_2 system (much more stable than the equivalent system derived from CuBP-H_2Me_2 and quite close to the CuBP-MeHMeH derived one, see Table 5) falls in between those computed for systems discussed above so that ΔG^{298K} for $(\text{reaction 1})_{DCM}$ shows an almost linear dependence on %Me (see solid squares in Figure 5); this suggests that the reactivity of such systems toward tButOOH could be finely tuned by percentage of substitution at precise positions of 2,2′-bpy ligands.

Another interesting observation that comes from the data reported in Figure 5, where solid circles represent ΔE and ΔG^{298K} for $(\text{reaction 2})_{DCM}$, is that the $[CuO]^+$ moiety formation (see Figure S4 for the computed UV−vis spectra) always resulted to be a less favored process than $[Cu(OH)]^+$, this being particular evident for Me = 0% and for Me = 50% (see Table 6), so suggesting that the selectivity toward possible oxygenated species can be tuned by percentage Me substitution too. Also for $[CuO]^+$ formation, the contribution

Table 4. Energetics and Thermodynamics (298 K) Features Computed for $(\text{reaction 1})_{DCM}$[a]

X_mY_n	ΔE	ΔH^{298K}	ΔG^{298K}	$-T\Delta S^{298K}$
Me_0H_4	−32.5	−37.7	−36.3	1.3
Me_2H_2	−8.1	−13.8	−9.3	4.5
Me_4H_0	17.2	13.0	24.0	11.0

[a]X = Me, Y = H. All quantities are reported in kJ mol^{-1}. $(\text{reaction 1})_{DCM}$: CuBP-$X_mY_n$ + tButOOH → Cu(OH)BP-X_mY_n + tButO.

Table 5. Energetics and Thermodynamics (298 K) Features of Cu(OH)BP-XYXY and Cu(OH)BP-Y_2X_2 Complexes Computed with Respect to Cu(OH)BP-X_2Y_2[a]

X_mY_n	ΔE	ΔH^{298K}	ΔG^{298K}	$-T\Delta S^{298K}$
Me_2H_2	0.0	0.0	0.0	0.0
MeHMeH	0.4	1.4	2.4	1.0
H_2Me_2	6.2	5.3	16.3	11.1

[a]X = Me, Y = H. All quantities are reported in kJ mol^{-1}.

https://doi.org/10.1021/acsomega.4c00598
ACS Omega 2024, 9, 16610−16620

Table 6. Energetics and Thermodynamics (298 K) Features Computed for (reaction 2)$_{DCM}$[a]

X_mY_n	ΔE	ΔH^{298K}	ΔG^{298K}	$-T\Delta S^{298K}$
Me_0H_4	−14.7	−15.5	−10.8	4.7
Me_2H_2	6.4	2.5	11.2	8.6
Me_4H_0	22.1	21.5	28.4	6.9

[a]X = Me, Y = H. All quantities are reported in kJ mol^{-1}. (reaction 2)$_{DCM}$: CuBP-X_mY_n + tButOOH → Cu(O)BP-X_mY_n + tButOH.

from dispersive interactions resulted in playing a fundamental role in determining the final ΔE ($\Delta E_{D3\text{-}bj}$ of −18.1, −15.6, and −18.7 kJ mol^{-1} were computed for Cu(O)BP-Me_0H_4, Cu(O)BP-Me_2H_2, and Cu(O)BP-Me_4H_0, respectively; ΔE_{el} shows also in this case a good linear correlation with %Me (see Figure S5 and Table S3).

Finally, to verify that the obtained ΔE vs %Me linear correlation is not just due to the adopted DFT functional (B3LYP-D3-bj in this case), the energetics of (reaction 1)$_{DCM}$ were computed (see the Theoretical Basis Section for further details) through the adoption of several DFT-based functionals other than the B3LYP-D3-bj one: even if strong dependence of the intercept (average = −33.2 kJ mol^{-1}, min = −10 kJ mol^{-1}, max = −68.7 kJ mol^{-1}) from the adopted functional was obtained (see Table S4 for further details), the linear trend was nicely reproduced in all cases, with the slope (expressed in kJ mol^{-1} %Me^{1-}) being less affected and varying in between min = 0.426 and max = 0.580 (average = 0.493). The origin of the obtained variation in the intercept value for (reaction 1)$_{DCM}$ between the adopted DFT-based functionals can be partially understood by examining the data reported in Table S6, where contributions (computed along the reported subreactions composing (reaction 1)$_{DCM}$, see Tables S5 and S6) to total ΔE are reported. As can be seen, ΔE_1 (i.e., the computed energy cost for breaking the O−O bond of tBuOOH, see Table S6)[14] and ΔE_{int} (i.e., the computed energy gain when the Cu−OH bond is formed, see Table S6) resulted to be particularly affected by the choice of the functional (B3LYP-D3-bj vs M06-D3 and M062x-D3). Such dependence is connected to different treatments of exchange and correlation typical for each adopted functional: it is so clear that to reach a conclusive answer where the intercept falls, more sophisticated *ab initio* methods should be used, this being however out of the scope of the present paper. In this respect, it has to be noticed here that the B_1 test (see the Theoretical Basis Section for its definition) gave indication that the investigated systems here, at variance with respect to isolated $[CuOH]^+$ (B_1 = 13.8 kcal mol^{-1} and T_1 = 0.05 with ρ_{Cu} = 0.242 *e*), should not be characterized by high static correlation and a strong multi-reference character (B_1 = 0.8 kcal mol^{-1} and B_1 = 1.7 kcal mol^{-1} for Cu(OH)BP-Me_0H_4 and Cu(OH)BP-Me_4H_0, respectively); this supports the hypothesis that the hybrid functional, quite useful in providing spectroscopic data, does not introduce too much error[15] in the evaluation of energetics characterizing the considered reactions. For the sake of comparison, the B_1 test was also performed on Cu(O)BP-Me_0H_4; this time it resulted to be B_1 = 7.6 kcalmol^{-1}, i.e., significantly lower than the value obtained in this work for isolated $[CuO]^+$ (B_1 = 18.5 kcal mol^{-1} and T_1 = 0.05 with ρ_{Cu} = 0.231 *e*),[16−18] but it however suggests that the systems containing the $[CuO]^+$ moiety have to be considered with care. Calculations of ΔE_{int} (see Table S5 for its definition) performed at B3LYP-D3-bj (ΔE_{int} = −234.7 kJ mol^{-1}), M06-D3 (ΔE_{int} = −217.8 kJ mol^{-1}), and M062x-D3 (ΔE_{int} = −253.4 kJ mol^{-1}) levels confirmed however the trend already obtained for the Cu(OH)BP-Me_0H_4 system (see Table S6).

CONCLUSIONS

In this paper, data from cyclic voltammetry and a DFT (B3LYP plus dispersive interactions treated through the empirical D3-bj scheme and implicit solvent as defined in the Gaussian16 code, see the Theoretical Basis Section) computational study on redox behaviour and reactivity of $[2,2'\text{-bpy}]_2$ Cu^+ containing homoleptic complexes toward tBuOOH as a function of the degree of substitution (%Me) by methyl groups at the 6,6' position were presented. As far as cyclic voltammetry results are concerned, a linear correlation was observed between %Me and reduction potentials, being located at +0.17(−5.27), −0.12(−4.98) and −0.45(−4.65) V(eV) vs Fc^+/Fc(vacuum) for %Me = 100%, %Me = 50%, and %Me = 0%, respectively, and a quite good reversibility for %Me = 100% and %Me = 50% was observed. Also, computed (B3LYP-D3bj and PCM scheme) reduction potentials vs vacuum resulted to be in good agreement with the experimental ones.

As far as the reactivity toward tBuOOH is concerned, B3LYP-D3bj and PCM schemes were adopted to investigate in a systematic way how the properties (both geometric and electronic through the calculation of UV−vis spectra) of the formed Cu(OH) and CuO are influenced by the percentage of substitution by methyl groups (%Me) of 2,2'-bpy ligands at the 6,6' position. Also, energetics and thermodynamics features concerning their formation were investigated in depth.

From the presented data, it is clearly shown that %Me substitution can be used to finely tune the properties of $[CuOH/O]^+$ species (in which Cu is in the +2 oxidation state as resulting from spin density analysis); in particular, the inspection of the obtained geometrical features of complexes Cu(OH)BP-Me_0H_4, Cu(OH)BP-Me_2H_2 (OH/O in the *cis* position with respect Me groups), and Cu(OH)BP-Me_4H_0 (where %Me substitution runs from 0 to 100%, through 50%) showed that for %Me = 0, Cu^{2+} resulted to be in a sort of square planar coordination (as expected for Cu^{2+} species) when OH and three N atoms from 2,2'-bpy ligands are considered. On passing to species obtained for %Me = 50 and %Me = 100%, Cu^{2+} maintains a C_{2v}-like coordination. This is reflected quite clearly in the computed UV−vis spectra for the three systems. When $[CuO]^+$ species are considered, the same conclusions can be drawn.

When energetics and thermodynamics features about the formation of $[Cu(OH)/O]^+$ from tBuOOH along (reaction 1)$_{DCM}$ and (reaction 2)$_{DCM}$ (see the Theoretical Basis Section for their definition) are of concern, a good linear correlation between the computed $\Delta E/\Delta G^{298K}$ and %Me substitution was obtained, with $[CuOH]^+$ being the most affected. Also, reaction 1 turned out to be the most favored one, in particular when %Me = 0 and %Me = 50%, suggesting that the selectivity toward possible Cu oxygenated species can be tuned by altering the %Me.

MATERIALS AND METHODS

Synthetic Procedures and NMR Characterization. All chemicals and solvents used were employed without further purification. If not differently specified, all the materials were purchased from Sigma-Aldrich. The 2,2'-bipyridil ligand

https://doi.org/10.1021/acsomega.4c00598
ACS Omega 2024, 9, 16610−16620

(purity ≥ 98%) and 6,6′-dimethyl-2,2'bipyridil ligand (purity ≥ 98%) are commercially available, while the 6-methyl-2,2'bipyridil ligand was synthesized adopting a literature procedure[19] as described below. For the synthesis of the 6-methyl-2,2'bipyridil ligand, octanol of ACS spectrophotometer grade (≥ 99%) was purchased from Sigma-Aldrich and the Nickel Raney catalyst was purchased from Sigma-Aldrich as W.R. Grace and Co. Raney 2800, slurry, in H_2O, active catalyst. For the washing procedure, absolute ethanol (HPLC grade < 99.8%) was used. Newly synthesized compounds were purified (when specified) through chromatography by using a Biotage SP1 Flash Chromatograph in direct phase using a Biotage Sfar Silica D-Duo 60 μm column. All the Cu(I) complexes were synthesized by using the general procedure reported below and previously reported.[5] Synthesis and characterization of $[Cu(2,2'\text{-}6,6'\text{-}Me_2\text{-}bpy)_2]^+[PF_6]^-$ and $[Cu(2,2'\text{-}bpy)_2]^+[PF_6]^-$ were previously reported by our group.[5]

The NMR spectra were recorded on a Jeol ECZ-R 600 MHz instrument, in deuterated acetone, using the residual solvent peak as an internal reference 1H: 2.05 ppm.[20] The chemical shifts are reported in delta (δ) units. Coupling constants are reported in Hertz (Hz). Multiplicity is reported as follows: s (singlet), d (doublet), t (triplet), and m (multiplet). For the experiment, eight scans were used with a relaxation of 5 s and an acquisition time of 2.9 s.

Synthesis of 6-Methyl-2,2′-bipyridine. The Ni Raney catalyst (5 g, including storage water) was first treated to remove the water. At this scope, the catalyst was washed 2 times with ethanol (20 mL) and one last time with the reaction solvent octanol (20 mL). At this point, octanol (25 mL) was added to the Ni Raney in a round-bottom flask, and 2,2′-bipyridine (1.87 g, 12 mmol) was added to the mixture that was stirred for 48 h at reflux. After that, the solution was filtered to remove the catalyst and the filtrate was treated with HCl 2 M to extract the product from the octanol. The obtained aqueous phase was then basified with NaOH (1 M aqueous solution) and extracted 3 times with 25 mL of dichloromethane. The organic phases containing the product were dried over magnesium sulfate, and dichloromethane was removed under reduced pressure. The final product was afforded after chromatographic purification (hexane:ethyl acetate/8:2). The NMR is compatible with a previous report.[19]

^{1}H NMR (600 MHz, chloroform-d) δ 8.66 (ddd, J = 4.8, 1.8, 0.9 Hz, 1H), 8.38 (dt, J = 8.0, 1.1 Hz, 1H), 8.15 (ddq, J = 7.8, 1.1, 0.6 Hz, 1H), 7.79 (ddd, J = 8.0, 7.5, 1.8 Hz, 1H), 7.69 (t, J = 7.7 Hz, 1H), 7.27 (ddd, J = 7.5, 4.8, 1.2 Hz, 1H), 7.26 (solvent residual peak), 7.16 (ddt, J = 7.7, 1.0, 0.5 Hz, 1H), 2.62 (s, 1H).

General Procedure for $[Cu(2,2'\text{-}S\text{-}bpy)_2][PF_6]$ Complexes. The $[Cu(2,2'\text{-}S\text{-}bpy)_2][PF_6]$ series was synthesized following a literature report[21] by mixing tetrakis(acetonitrile)-copper(I) hexafluorophosphate (1 mmol) and the bipyridine ligand (2.1 mmol) in anhydrous dichloromethane (0.1 M). The solution was stirred under a N_2 atmosphere for 3 h at room temperature, and after stripping the solvent, a powder was obtained. The powder was then washed several times with a 1:1 mixture of diethyl ether and petroleum ether and dried to obtain the final product. The complexes were obtained in an excellent yield ranging from 94 to 97%.

Synthesis of $[Cu(2,2'\text{-}6\text{-}Me\text{-}bpy)_2]^+[PF_6]^-$. Following the general procedure, $[Cu(2,2'\text{-}6\text{-}Me\text{-}bpy)_2]^+[PF_6]^-$ was obtained with 95% yield. The NMR shifts are reported below (see Figure S5 for NMR spectrum).

^{1}H NMR (600 MHz, acetone-d_6) δ 8.71 (ddd, J = 5.1, 1.7, 0.9 Hz, 1H), 8.68 (dt, J = 8.2, 1.0 Hz, 1H), 8.52 (d, J = 8.0 Hz, 1H), 8.26 (ddd, J = 8.2, 7.5, 1.6 Hz, 1H), 8.17 (t, J = 7.8 Hz, 1H), 7.71 (ddd, J = 7.6, 5.1, 1.1 Hz, 1H), 7.66 (d, J = 7.7 Hz, 1H), 2.33 (s, 3H), 2.05 (solvent residual peak).

Cyclic Voltammetry Measurements. Cyclic voltammetry profiles were recorded by using a SP-150 potentiostat (Biologic) in a three-electrode setup configuration using a glassy carbon (diameter 1 cm) as a working electrode, a platinum wire as a counter-electrode, and a Ag^+/Ag reference electrode, with a scan rate as high as 100 mV s^{-1}. Copper complexes in their pristine Cu(I) form (final concentration in solution of 0.001 M) were dissolved in a 0.1 M solution of $TBA^+PF_6^-$ (as a supporting electrolyte) in DCM. Moreover, ferrocene was used as an internal standard in all the measurements. Redox potentials were obtained as the semisum ($E_{1/2}$) of the potential values at the maximum of the peaks in the oxidation and reduction scans. All the potential values were referred to the Fc^+/Fc redox potential by applying the following equation:

$$E[\text{V vs } Fc^+/Fc] = E[\text{V vs } Ag^+/Ag] - 0.51 \text{ V}$$

From E [V vs Fc^+/Fc] redox potential, values referring to vacuum (E vs vacuum and/or E_{exp} vs vacuum in eV) were obtained by applying the following equation:

$$E[\text{eV}]\text{vs vacuum} = -(5.1 \text{ V} + E[\text{V vs } Fc^+/Fc])$$

Raman Measurements. Raman measurements were performed on a Renishaw Raman Microscope (In Via system) adopting a He−Cd 442 nm exciting laser line (EEL); EEL was focused on the sample through a 20× ultralong-working-distance objective through which the resulting backscattered light was then sent to a 2400 l mm^{-1} grating analyzer and then to a CCD detector. The sample was constituted by an adapted Helma glass cuvette (QS grade, 1 cm optical path) filled by DCM solution of $[Cu(2,2'\text{-}\boldsymbol{6\text{-}Me}\text{-}bpy)_2]^+[PF6]^-$/$[Cu(2,2'\text{-}\boldsymbol{6,6'\text{-}Me_2}\text{-}bpy)_2]^+[PF6]^-$ (1×10^{-3} M concentration) with magnetic stirring. The stability of the sample under laser light (10% of the total power, less than 1 mW) was checked. The presented spectra correspond to the average of three spectra obtained by accumulating 20 acquisitions, each one with a duration of 20 s (20 × 20s).

Theoretical Basis. All the calculations (structure optimization, computation of vibrational frequencies, and UV−vis spectra) were performed by means of the Gaussian 16 code[22] at the B3LYP-D3-bj[23,24] level of theory (ultrafine grid is used for the integral evaluation) and adopting the unrestricted formalism for describing open-shell systems. TD-DFT[25] was adopted for computing electronic transitions (first 10 transitions) and the corresponding UV−vis spectra. The basis set for describing H, C, B, N, F, O, P, and Cu atoms was the standard Pople 6-31+G(2d,p). Finally, solvent (DCM) effects were included through the PCM (IEF-PCM) approach[26] as developed in the Gaussian16 code and without changing the default settings.

$[Cu(2,2'\text{-}bpy)_2]^+[PF6]^-$ (0% Me substitution), $[Cu(2,2'\text{-}6\text{-}Me\text{-}bpy)_2]^+[PF6]^-$ (50% Me substitution), and $[Cu(2,2'\text{-}6,6'\text{-}Me_2\text{-}bpy)_2]^+[PF6]^-$ (100% Me substitution) homoleptic complexes (Me = $-CH_3$) and their possible derivatives after interaction with tButOOH were modeled adopting the CuBP-X_mY_n model (see Figure 1 for its graphical representation) where X = Me, Y = H, and m, n = 0−4. According to this definition, three different cluster models can be identified: (a)

https://doi.org/10.1021/acsomega.4c00598
ACS Omega 2024, 9, 16610−16620

$CuBP\text{-}Me_0H_4$ (corresponding to $[Cu(2,2'\text{-bpy})_2]^+[PF6]^-$), (b) $CuBP\text{-}Me_2H_2$ (corresponding to $[Cu(2,2'\text{-6-Me-bpy})_2]^+[PF6]^-$, and (c) $CuBP\text{-}M_4H_0$ (corresponding to $[Cu(2,2'\text{-}6,6'\text{-}Me_2\text{-bpy})_2]^+[PF6]^-$). For the sake of brevity, the PF_6^- anion is excluded from the cluster model definition, but it is always included in calculations, so the total charge is set always to zero. Moreover, for the oxidized form of $CuBP\text{-}Me_2H_2$, three possible situations were investigated: (a) OH/O species in the *cis* position with respect to two Me groups (indicated in the following as $Cu(OH/O)BP\text{-}Me_2H_2$), (b) OH/O species in the *cis* position with respect to Me and H groups (indicated in the following as Cu(OH/O)BP-MeHMeH), and (c) OH/O species in the *cis* position with respect to two H groups (indicated in the following as $Cu(OH/O)BP\text{-}H_2Me_2$). Spin multiplicity was, respectively, set to 2S + 1 = 1 and 2S + 1 = 2 for $CuBP\text{-}X_mY_n$ and $Cu(OH)BP\text{-}X_mY_n$ and 2S + 1 = 3 for $Cu(O)BP\text{-}X_mY_n$ and $(tButO)Cu(OH)\text{-}X_mY_n$ molecular models, the final spin contamination always resulting to be less than 10%.

Computed E [ev] vs vacuum values (hereafter E_{comp}, to be compared with experimental values E_{exp} as above-defined) were obtained from ΔG_{red}^{298K} computed for the reaction:

$$Cu(II)BP\text{-}X_mY_n + e^- \rightarrow Cu(I)BP\text{-}X_mY_n$$

without including ΔH and $-T\Delta S$ for free electron and applying the PCM (IEF-PCM) approach[26] as an implicit solvent scheme. Two types of ΔG_{red}^{298K} were evaluated: (i) the first (hereafter ΔG_{red}^{298K}) was obtained by adopting the Gaussian16 code default settings for the PCM scheme from the relation $\Delta G_{red}^{298K} = G(Cu(I)BP\text{-}X_mY_n) - G(Cu(II)BP\text{-}X_mY_n)$ where G values were computed after frequency calculations on fully optimized structures; (ii) the second (hereafter ${}^{drc}\Delta G_{red}^{298K}$) obtained through the relation ${}^{drc}\Delta G_{red}^{298K} = {}^{drc}\Delta E_{red}^{298K} + {}^{corr}\Delta G_{red}^{298K}$; in this case, ${}^{drc}\Delta E_{red}^{298K}$ was obtained by single-point energy calculation on optimized structures obtained at point (i) and switching on the *dis*,[27,28] *rep*,[27,28] and *cav*[29] additional inputs for the PCM scheme; ${}^{corr}\Delta G_{red}^{298K}$ is the difference between the thermal correction to Gibbs free energy terms obtained from frequency calculation performed on structures at step (i).

To evaluate the energetics and thermodynamics features of the considered reactions (in DCM) among $CuBP\text{-}X_mY_n$ and tButOOH, i.e.:

$$(\text{reaction 1})_{DCM} = CuBP\text{-}X_mY_n + tButOOH \rightarrow Cu(OH)BP\text{-}X_mY_n + tButO$$

$$(\text{reaction 2})_{DCM} = CuBP\text{-}X_mY_n + tButOOH \rightarrow Cu(O)BP\text{-}X_mY_n + tButOH$$

ΔE, ΔH^{298K}, and ΔG^{298K} were computed according to the general formula:

$$\Delta E = \Sigma e_p - \Sigma e_r;\ \Delta H^{298K} = \Sigma h^{298K}{}_p - \Sigma h^{298K}{}_r;\ \Delta G^{298K} = \Sigma g^{298K}{}_p - \Sigma g^{298K} r$$

where e, h^{298K}, and g^{298K} refer to the electronic energy, enthalpy, and Gibbs free energy and r and p show, respectively, the reactants and products.

Moreover, ΔE for reaction 1 was also evaluated adopting the PBE0[30]-D3-bj,[12,13] M06L[31]-D3,[12] M06[32]-D3,[12] M062x[32]-D3,[12] TPSSh[33,34]-D3-bj,[35] cam-B3LYP[36]-D3-bj,[12,13] and ωB97X[37]-D3[35] functionals through single-point energies on optimized B3LYP-D3-bj geometries.

Finally, to test the degree of static correlation and the multireference character of the formed Cu−OH bond in $CuBP\text{-}X_mY_n$ complexes, the B_1 test proposed by Truhlar et al.[15] was adopted on $CuBP\text{-}Me_0H_4$ and $CuBP\text{-}Me_4H_0$, the energy contribution to binding energies BE being computed, respectively, on optimized $Cu(OH)BP\text{-}X_mY_n$, optimized OH, and $[CuBP\text{-}X_mY_n]_{def}$ (i.e., the $CuBP\text{-}X_mY_n$ complex in the geometry that it has after the interaction with OH). For systems/chemical bonds where static correlation and multireference character are negligible, B_1 was verified to be $B_1 < 10$ kcal mol^{-1}. Notice that B_1 (together with the T_1 diagnostic at the CCSD level)[38,39] was also computed on the isolated $(CuOH)^+$ / $(CuO)^+$ reference systems.

■ ASSOCIATED CONTENT

Supporting Information

The Supporting Information is available free of charge at https://pubs.acs.org/doi/10.1021/acsomega.4c00598.

Computed and experimental Raman spectra; computed UV−vis spectra; NMR spectra; ΔE_{el} vs %Me; energetics and thermodynamics features; computed fitting parameters; contributions to ΔE of $(\text{reaction 1})_{DCM}$ from subreactions; dependence of ΔE (computed for $CuBP\text{-}Me0H_4$) of $(\text{reaction 1})_{DCM}$ from the DFT functionals; dependence of contributions to ΔE of $(\text{reaction 1})_{DCM}$ from selected DFT functionals; *xyz* coordinates of the optimized structures (PDF)

■ AUTHOR INFORMATION

Corresponding Author

Alessandro Damin − *Department of Chemistry, NIS and INSTM Reference Centre, University of Turin, Turin 10135, Italy*; orcid.org/0000-0002-1110-0993; Email: alessandro.damin@unito.it

Authors

Matteo Bonomo − *Department of Chemistry, NIS and INSTM Reference Centre, University of Turin, Turin 10135, Italy*; orcid.org/0000-0002-1944-2664

Barbara Centrella − *Department of Chemistry, NIS and INSTM Reference Centre, University of Turin, Turin 10135, Italy*

Matteo Signorile − *Department of Chemistry, NIS and INSTM Reference Centre, University of Turin, Turin 10135, Italy*; orcid.org/0000-0003-0521-3702

Claudia Barolo − *Department of Chemistry, NIS and INSTM Reference Centre, University of Turin, Turin 10135, Italy*; orcid.org/0000-0003-0627-2579

Silvia Bordiga − *Department of Chemistry, NIS and INSTM Reference Centre, University of Turin, Turin 10135, Italy*; orcid.org/0000-0003-2371-4156

Complete contact information is available at: https://pubs.acs.org/10.1021/acsomega.4c00598

Notes

The authors declare no competing financial interest.

https://doi.org/10.1021/acsomega.4c00598
ACS Omega 2024, 9, 16610−16620

■ ACKNOWLEDGMENTS

The authors acknowledge the funding from Horizon 2020 Excellence Science ERC-Synergy program 2019-CUBE: "Unravelling the Secrets of Cu-Based Catalysts for C−H Activation" (grant agreement no. 856446). Authors acknowledge support from Project CH4.0 under the MUR program "Dipartimenti di Eccellenza 2023-2027" (CUP: D13C22003520001).

■ REFERENCES

(1) Keller, S.; Constable, E. C.; Housecroft, C. E.; Neuburger, M.; Prescimone, A.; Longo, G.; Pertegás, A.; Sessolo, M.; Bolink, H. J. [Cu(N^N)(P^P)]+ Containing Light-Emitting Electrochemical Cells: Improving Performance through Simple Substitution. *Dalton Transactions* **2014**, *43* (44), 16593−16596.

(2) Keller, S.; Pertegás, A.; Longo, G.; Martínez, L.; Cerdá, J.; Junquera-Hernández, J. M.; Prescimone, A.; Constable, E. C.; Housecroft, C. E.; Ortí, E.; Bolink, H. J. Shine Bright or Live Long: Substituent Effects in [Cu(N^N)(P^P)]+-Based Light-Emitting Electrochemical Cells Where N^N Is a 6-Substituted 2,2′-Bipyridine. *J. Mater. Chem. C Mater.* **2016**, *4* (17), 3857−3871.

(3) Keller, S.; Prescimone, A.; La Placa, M. G.; Junquera-Hernández, J. M.; Bolink, H. J.; Constable, E. C.; Sessolo, M.; Ortí, E.; Housecroft, C. E. The Shiny Side of Copper: Bringing Copper(i) Light-Emitting Electrochemical Cells Closer to Application. *RSC Adv.* **2020**, *10* (38), 22631−22644.

(4) Saygili, Y.; Söderberg, M.; Pellet, N.; Giordano, F.; Cao, Y.; Munoz-García, A. B.; Zakeeruddin, S. M.; Vlachopoulos, N.; Pavone, M.; Boschloo, G.; Kavan, L.; Moser, J. E.; Grätzel, M.; Hagfeldt, A.; Freitag, M. Copper Bipyridyl Redox Mediators for Dye-Sensitized Solar Cells with High Photovoltage. *J. Am. Chem. Soc.* **2016**, *138* (45), 15087−15096.

(5) Centrella, B.; Deplano, G.; Damin, A.; Signorile, M.; Tortora, M.; Barolo, C.; Bonomo, M.; Bordiga, S. A Multi-Technique Approach to Unveil the Redox Behaviour and Potentiality of Homoleptic CuI Complexes Based on Substituted Bipyridine Ligands in Oxygenation Reactions. *Dalton Transactions* **2022**, *51* (38), 14439−14451.

(6) Bozic-Weber, B.; Constable, E. C.; Housecroft, C. E.; Kopecky, P.; Neuburger, M.; Zampese, J. A. The Intramolecular Aryl Embrace: From Light Emission to Light Absorption. *Dalton Transactions* **2011**, *40* (46), 12584−12594.

(7) Bozic-Weber, B.; Chaurin, V.; Constable, E. C.; Housecroft, C. E.; Meuwly, M.; Neuburger, M.; Rudd, J. A.; Schönhofer, E.; Siegfried, L. Exploring Copper(i)-Based Dye-Sensitized Solar Cells: A Complementary Experimental and TD-DFT Investigation. *Dalton Transactions* **2012**, *41* (46), 14157−14169.

(8) Chermette, H. Chemical Reactivity Indexes in Density Functional Theory. *J. Comput. Chem.* **1999**, *20* (1), 129−154.

(9) Domingo, L. R.; Ríos-Gutiérrez, M.; Pérez, P. Applications of the Conceptual Density Functional Theory Indices to Organic Chemistry Reactivity. *Molecules* **2016**, *21* (6), 1−22.

(10) Tubbs, K. J.; Fuller, A. L.; Bennett, B.; Arif, A. M.; Berreau, L. M. Mononuclear N3S(Thioether)-Ligated Copper(II) Methoxide Complexes: Synthesis, Characterization, and Hydrolytic Reactivity. *Inorg. Chem.* **2003**, *42* (16), 4790−4791.

(11) Christensen, E. G.; Lutz, K. T.; Steele, R. P. Electronic Structure and Vibrational Signatures of the Delocalized Radical in Hydrated Clusters of Copper("II") Hydroxide Cuoh+(H2o)0−2. *J. Phys. Chem. A* **2021**, *125* (17), 3631−3645.

(12) Grimme, S.; Antony, J.; Ehrlich, S.; Krieg, H. A Consistent and Accurate Ab Initio Parametrization of Density Functional Dispersion Correction (DFT-D) for the 94 Elements H-Pu. *J. Chem. Phys.* **2010**, *132* (15), 154104 DOI: 10.1063/1.3382344.

(13) Grimme, S.; Ehrlich, S.; Goerigk, L. Effect of the Damping Function in Dispersion Corrected Density Functional Theory. *J. Comput. Chem.* **2011**, *32* (7), 1456−1465.

(14) Bach, R. D.; Schlegel, H. B. Bond Dissociation Energy of Peroxides Revisited. *J. Phys. Chem. A* **2020**, *124* (23), 4742−4751.

(15) Schultz, N. E.; Zhao, Y.; Truhlar, D. G. Density Functional for Inorganometallic and Organometallic Chemistry. *J. Phys. Chem. A* **2005**, *109* (49), 11127−11143.

(16) Srnec, M.; Navrátil, R.; Andris, E.; Jašík, J.; Roithová, J. Experimentally Calibrated Analysis of the Electronic Structure of CuO +: Implications for Reactivity. *Angewandte Chemie - International Edition* **2018**, *57* (52), 17053−17057.

(17) Nakao, Y.; Hirao, K.; Taketsugu, T. Theoretical Study of First-Row Transition Metal Oxide Cations. *J. Chem. Phys.* **2001**, *114* (18), 7935−7940.

(18) Rezabal, E.; Gauss, J.; Matxain, J. M.; Berger, R.; Diefenbach, M.; Holthausen, M. C. Quantum Chemical Assessment of the Binding Energy of CuO+. *J. Chem. Phys.* **2011**, *134* (6), No. 064304, DOI: 10.1063/1.3537797.

(19) Bröring, M.; Kleeberg, C. Convenient Procedure for the α-Methylation of Simple Pyridines. *Synth. Commun.* **2008**, *38* (21), 3672−3682.

(20) Gottlieb, H. E.; Kotlyar, V.; Nudelman, A. NMR Chemical Shifts of Common Laboratory Solvents as Trace Impurities. *J. Org. Chem.* **1997**, *62* (21), 7512−7515.

(21) Giordano, M.; Volpi, G.; Bonomo, M.; Mariani, P.; Garino, C.; Viscardi, G. Methoxy-Substituted Copper Complexes as Possible Redox Mediators in Dye-Sensitized Solar Cells. *New J. Chem.* **2021**, *45* (34), 15303−15311.

(22) Frisch, M. J.; Trucks, G. W.; Schlegel, H. B.; Scuseria, G. E.; Robb, M. A.; Cheeseman, J. R.; Scalmani, G.; Barone, V.; Petersson, G. A.; Nakatsuji, H.; Li, X.; Caricato, M.; Marenich, A. V.; Bloino, J.; Janesko, B. G.; Gomperts, R.; Mennucci, B.; Hratchian, H. P.; Ortiz, J. V.; Izmaylov, A. F.; Sonnenberg, J. L.; Williams-Young, D.; Ding, F.; Lipparini, F.; Egidi, F.; Goings, J.; Peng, B.; Petrone, A.; Henderson, T.; Ranasinghe, D.; Zakrzewski, V. G.; Gao, J.; Rega, N.; Zheng, G.; Liang, W.; Hada, M.; Ehara, M.; Toyota, K.; Fukuda, R.; Hasegawa, J.; Ishida, M.; Nakajima, T.; Honda, Y.; Kitao, O.; Nakai, H.; Vreven, T.; Throssell, K.; Montgomery, Jr., J. A.; Peralta, J. E.; Ogliaro, F.; Bearpark, M. J.; Heyd, J. J.; Brothers, E. N.; Kudin, K. N.; Staroverov, V. N.; Keith, T. A.; Kobayashi, R.; Normand, J.; Raghavachari, K.; Rendell, A. P.; Burant, J. C.; Iyengar, S. S.; Tomasi, J.; Cossi, M.; Millam, J. M.; Klene, M.; Adamo, C.; Cammi, R.; Ochterski, J. W.; Martin, R. L.; Morokuma, K.; Farkas, O.; Foresman, J. B.; Fox, D. J. *Gaussian 16, Revision B.01*. Gaussian, Inc.: Wallingford CT,2016.

(23) Becke, A. D. Density-functional Thermochemistry. III. The Role of Exact Exchange. *J. Chem. Phys.* **1993**, *98*, 5648−5652.

(24) Lee, C.; Yang, W.; Parr, R. G. Development of the Colle-Salvetti Correlation-Energy Formula into a Functional of the Electron Density. *Phys. Rev. B* **1988**, *37*, 785−789.

(25) Adamo, C.; Jacquemin, D. The Calculations of Excited-State Properties with Time-Dependent Density Functional Theory. *Chem. Soc. Rev.* **2013**, *42* (3), 845−856.

(26) Tomasi, J.; Mennucci, B.; Cammi, R. Quantum Mechanical Continuum Solvation Models. *Chem. Rev.* **2005**, *105* (8), 2999−3093.

(27) Floris, F.; Tomasi, J. Evaluation of the Dispersion Contribution to the Solvation Energy. A Simple Computational Model in the Continuum Approximation. *J. Comput. Chem.* **1989**, *10* (5), 616−627.

(28) Floris, F. M.; Tomasi, J.; Ahuir, J. L. P. Dispersion and Repulsion Contributions to the Solvation Energy: Refinements to a Simple Computational Model in the Continuum Approximation. *J. Comput. Chem.* **1991**, *12* (7), 784−791.

(29) Pierotti, R. A. A Scaled Particle Theory of Aqueous and Nonaqueous Solutions. *Chem. Rev.* **1976**, *76* (6), 717−726.

(30) Adamo, C.; Barone, V. Toward Reliable Density Functional Methods without Adjustable Parameters: The PBE0Model. *J. Chem. Phys.* **1999**, *110* (13), 6158−6170.

(31) Zhao, Y.; Truhlar, D. G. A New Local Density Functional for Main-Group Thermochemistry, Transition Metal Bonding, Thermochemical Kinetics, and Noncovalent Interactions. *J. Chem. Phys.* **2006**, *125* (19), 194101 DOI: 10.1063/1.2370993.

https://doi.org/10.1021/acsomega.4c00598
ACS Omega 2024, 9, 16610−16620

(32) Zhao, Y.; Truhlar, D. G. The M06 Suite of Density Functionals for Main Group Thermochemistry, Thermochemical Kinetics, Noncovalent Interactions, Excited States, and Transition Elements: Two New Functionals and Systematic Testing of Four M06-Class Functionals and 12 Other Functionals. *Theor. Chem. Acc.* **2008**, *120* (1−3), 215−241.
(33) Staroverov, V. N.; Scuseria, G. E.; Tao, J.; Perdew, J. P. Comparative Assessment of a New Nonempirical Density Functional: Molecules and Hydrogen-Bonded Complexes. *J. Chem. Phys.* **2003**, *119* (23), 12129−12137.
(34) Staroverov, V. N.; Scuseria, G. E.; Tao, J.; Perdew, J. P. Erratum: Comparative Assessment of a New Nonempirical Density Functional: Molecules and Hydrogen-Bonded Complexes(Journal of Chemical Physics (2003) 119 (12129)). *J. Chem. Phys.* **2004**, *8*, 11507.
(35) Goerigk, L.; Hansen, A.; Bauer, C.; Ehrlich, S.; Najibi, A.; Grimme, S. A Look at the Density Functional Theory Zoo with the Advanced GMTKN55 Database for General Main Group Thermochemistry, Kinetics and Noncovalent Interactions. *Phys. Chem. Chem. Phys.* **2017**, *19* (48), 32184−32215.
(36) Yanai, T.; Tew, D. P.; Handy, N. C. A New Hybrid Exchange-Correlation Functional Using the Coulomb-Attenuating Method (CAM-B3LYP). *Chem. Phys. Lett.* **2004**, *393* (1−3), 51−57.
(37) Chai, J. D.; Head-Gordon, M. Systematic Optimization of Long-Range Corrected Hybrid Density Functionals. *J. Chem. Phys.* **2008**, *128* (8), No. 084106, DOI: 10.1063/1.2834918.
(38) Lee, T. J.; Taylor, P. R. A Diagnostic for Determining the Quality of Single-reference Electron Correlation Methods. *Int. J. Quantum Chem.* **1989**, *36* (23S), 199−207.
(39) Čížek, J. On the Use of the Cluster Expansion and the Technique of Diagrams in Calculations of Correlation Effects in Atoms and Molecules. *Adv. Chem. Phys.* **2007**, 35−89, DOI: 10.1002/9780470143599.ch2.

https://doi.org/10.1021/acsomega.4c00598
ACS Omega 2024, 9, 16610−16620